Kinetics of vascular normalization by VEGFR2 blockade governs brain tumor response to radiation: Role of oxygenation, angiopoietin-1, and matrix metalloproteinases

Frank Winkler,[1,3] Sergey V. Kozin,[1,3] Ricky T. Tong,[1] Sung-Suk Chae,[1] Michael F. Booth,[1] Igor Garkavtsev,[1] Lei Xu,[1] Daniel J. Hicklin,[2] Dai Fukumura,[1] Emmanuelle di Tomaso,[1] Lance L. Munn,[1] and Rakesh K. Jain[1,*]

[1]E.L. Steele Laboratory for Tumor Biology, Department of Radiation Oncology, Massachusetts General Hospital and Harvard Medical School, 100 Blossom Street, Boston, Massachusetts 02114
[2]ImClone Systems Incorporated, 180 Varick Street, New York, New York 10014
[3]These authors contributed equally to this work.
*Correspondence: jain@steele.mgh.harvard.edu

Summary

The recent landmark Phase III clinical trial with a VEGF-specific antibody suggests that antiangiogenic therapy must be combined with cytotoxic therapy for the treatment of solid tumors. However, there are no guidelines for optimal scheduling of these therapies. Here we show that VEGFR2 blockade creates a "normalization window"—a period during which combined radiation therapy gives the best outcome. This window is characterized by an increase in tumor oxygenation, which is known to enhance radiation response. During the normalization window, but not before or after it, VEGFR2 blockade increases pericyte coverage of brain tumor vessels via upregulation of Ang1 and degrades their pathologically thick basement membrane via MMP activation.

Introduction

Attempts to combine antiangiogenic therapy with radiation therapy have produced inconsistent findings: some experimental studies have demonstrated an additive tumor growth delay, others have shown a stronger, synergistic effect (Teicher et al., 1995; Mauceri et al., 1998; Lee et al., 2000; Kozin et al., 2001; Wachsberger et al., 2003), and one study showed a compromised therapeutic response (Murata et al., 1997). Moreover, previous studies have disagreed on the order in which antiangiogenic and radiation therapies should be given (Gorski et al., 1998; Rofstad et al., 2003; Zips et al., 2003). To design an optimum combination therapy, we must unravel the mechanism and timing of tumor vessel response to antiangiogenic agents and use this knowledge to optimize the treatment schedule.

Tumor vessels are structurally and functionally abnormal, with defective endothelium, basement membrane, and pericyte coverage (Carmeliet and Jain, 2000; Dvorak, 2002). These abnormalities impair the delivery of oxygen and therapeutics (Jain, 2003). One extreme example is glioblastoma multiforme, an invariably fatal brain tumor characterized by a dilated, tortuous, disorganized, and leaky vasculature and by high levels of VEGF (Plate et al., 1992; Millauer et al., 1994). Extensive hypoxia makes this highly malignant tumor resistant to radiation therapy (Rampling et al., 1994). In theory, reducing or abolishing vascular abnormalities by anti-VEGF therapy should "normalize" the tumor vasculature and alleviate hypoxia (Jain, 2001). On the other hand, extensive destruction of tumor vessels by antiangiogenic therapy can also hinder the delivery of oxygen and drugs, as reported in cases where the antiangiogenic agent TNP-470 was combined with radiation (Murata et al., 1997) and chemotherapy (Ma et al., 2001). It is therefore critical to determine how to combine these therapies optimally.

Here we characterize the time course of morphological, functional, and molecular changes in the vasculature of orthotopic gliomas in response to treatment with DC101, a monoclonal antibody against VEGFR2 (Flk-1), and the relationship between these vascular changes, tumor hypoxia, and radiation response. We show that it is possible to normalize the morphology and function of brain tumor vasculature for a period of time, leading to transient improvements in tumor oxygenation and response to radiation therapy. We also provide novel insight

SIGNIFICANCE

Most antiangiogenic cancer therapies focus on the destruction of solid tumors by eradication of their supporting vasculature. However, only combinations of antiangiogenic and chemotherapeutic agents have produced positive results in Phase III clinical trials. Preclinical models have shown that radiation therapy is likewise often more effective when combined with antiangiogenic therapy. The success of combination therapy may rely on the fact that antiangiogenic agents not only reduce the vessel density in tumors, but—at least temporarily—also improve the aberrant morphology of the remaining tumor vessels, resulting in a more efficient vasculature which is more similar to that of normal tissue. The time course of this "vascular normalization" should be taken into account when radiation and antiangiogenic therapy are combined.

into the role of angiopoietin-1 and matrix metalloproteinases in the normalization process.

Results

Anti-VEGFR2 therapy produces a time window of greatly reduced tumor hypoxia, during which radiation therapy is most effective

We conducted a systematic evaluation of five treatment schedules, using a combination of DC101 (a VEGFR2-specific monoclonal antibody) and γ radiation to treat human glioblastoma xenografts growing orthotopically in the mouse brain (Figure 1A). In patients, radiation (along with surgery) is the main treatment for these tumors. We found that, when used as a monotherapy, DC101 (given at 40 mg/kg on days 0, 3, and 6) produced a small, statistically insignificant tumor growth delay of ~2.5 days, while radiation (three daily fractionated doses of 7 Gy each) significantly delayed the growth by ~12.5 days. When DC101 was given in nonoptimal combinations with radiation (RT1, RT2, RT3, RT5), the combined therapy had no more than an additive effect. However, giving radiation therapy on days 4 to 6 after DC101 treatment began (RT4) produced a synergistic effect in which the tumor growth delay significantly exceeded the expected additive effect (Figure 1A).

Because hypoxia significantly decreases the efficacy of radiotherapy (Hall, 2000) and is typically severe in glioblastoma multiforme (Rampling et al., 1994), we hypothesized that this synergy arises from a DC101-induced improvement in tumor oxygenation, which enhances the cytotoxic effect of radiation treatment. Indeed, the optimum time for radiation treatment coincided with the time of maximum tumor oxygenation: during DC101 treatment, tumor hypoxia began to drop on day 2, was almost abolished on day 5, and increased again by day 8 (Figure 1B). In contrast, apoptosis of tumor and vascular cells did not coincide with the optimum treatment schedule: the apoptotic level increased significantly on day 5 and remained the same on day 8. Even at these times, apoptosis was moderate and did not lower the cellular (nuclear) density in tumor sections (Table 1). Thus, it is unlikely that increased tumor or vascular cell apoptosis after DC101 accounts for the reduced tumor hypoxia and the improved radiation response around day 5.

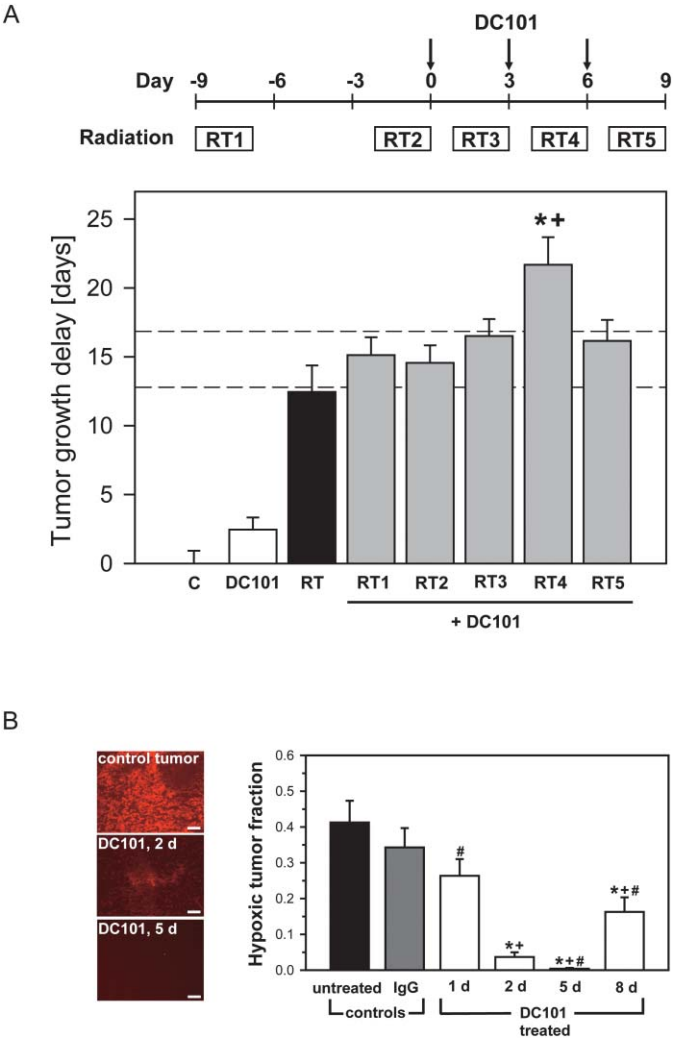

Figure 1. A combination of radiation and antiangiogenic therapies is only synergistic during a "normalization window" when tumor hypoxia is greatly diminished

A: Tumor growth delay of orthotopic U87 gliomas is shown for untreated controls (C), monotherapy with the VEGFR2-specific antibody DC101 (three injections, three days apart), local radiation for three consecutive days (RT), and five different combination schedules where radiation was given before, during, or after DC101 therapy (RT1–RT5; see diagram for schedules). The dashed lines show the range of the expected additive effect (EAE) of DC101 and radiation. *$p < 0.05$, compared to RT; $^{+}p < 0.05$, compared to EAE.

B: Tumor hypoxia (pimonidazole staining, red) was severe in control tumors, but decreased for a limited time during monotherapy with DC101. Hypoxia reached a minimum at day 5, and a partial relapse occurred at day 8. *$p < 0.05$, compared to untreated control; $^{+}p < 0.05$, compared to rat IgG-treated control (day 2); #$p < 0.05$, compared to day 2 after initiation of DC101 therapy.

Pericytes are recruited to existing tumor blood vessels during the normalization window, but not before or afterward

We set out to determine the mechanism by which VEGFR2 blockade transiently lowers hypoxia in glioma xenografts. We have shown that VEGF blockade can normalize the vasculature in transplanted (Yuan et al., 1996; Kadambi et al., 2001; Tong et al., 2004) and spontaneous human (Willett et al., 2004) tumors, decreasing the density, diameter, and tortuosity of vessels and improving their integrity. It is possible that vascular normalization can enhance the effectiveness of radiotherapy or chemotherapy by improving the delivery of oxygen and drugs, respectively (Jain, 2001). We therefore asked whether the alleviation of tumor hypoxia is due to the transient normalization of glioma vessels by anti-VEGFR2 therapy.

It has recently been demonstrated, in both murine and human tumors, that VEGF signal blockade increases the fraction of vessels that are covered with closely attached perivascular cells (Tong et al., 2004; Willett et al., 2004; Inai et al., 2004), but the time course of this change has not been determined to date. We found that, during DC101 treatment, vessel coverage by closely associated pericytes remained low through day 1, increased markedly between days 2 and 5, and fell again by day 8 (Figure 2A). Thus, the kinetics of pericyte coverage mirrored those of tumor hypoxia.

The mechanisms responsible for the increase in pericyte coverage are largely unknown. It is widely assumed that this

Table 1. Apoptosis in U87 gliomas after VEGFR2 blockade

	Untreated control	IgG-treated control	DC101 1 day	DC101 2 days	DC101 5 days	DC101 8 days
Nuclear density (nuclei/mm^2)	3166 ± 271	3214 ± 459	3181 ± 167	3315 ± 405	3503 ± 115	3142 ± 199
Apoptotic nuclei (% of total nuclei)	0.81 ± 0.09	0.86 ± 0.24	0.69 ± 0.05	0.67 ± 0.09	2.50 ± 0.31*$^{+\#}$	2.27 ± 0.23*$^{+\#}$
Vessel-associated apoptotic nuclei/mm^2	1.63 ± 0.59	0.91 ± 0.69	1.59 ± 0.30	0.94 ± 0.44	4.76 ± 0.90*$^{+\#}$	4.99 ± 1.03*$^{+\#}$

Quantification of nuclear density, total number of apoptotic nuclei, and vessel-associated apoptotic nuclei in control animals and at different time points after treatment with 40 mg/kg DC101 (days 0, 3, and 6). *$p < 0.05$, compared to untreated controls; $^{+}p < 0.05$, compared to control-IgG treated animals (day 2); $^{\#}p < 0.05$, compared to DC101-treated animals (day 2).

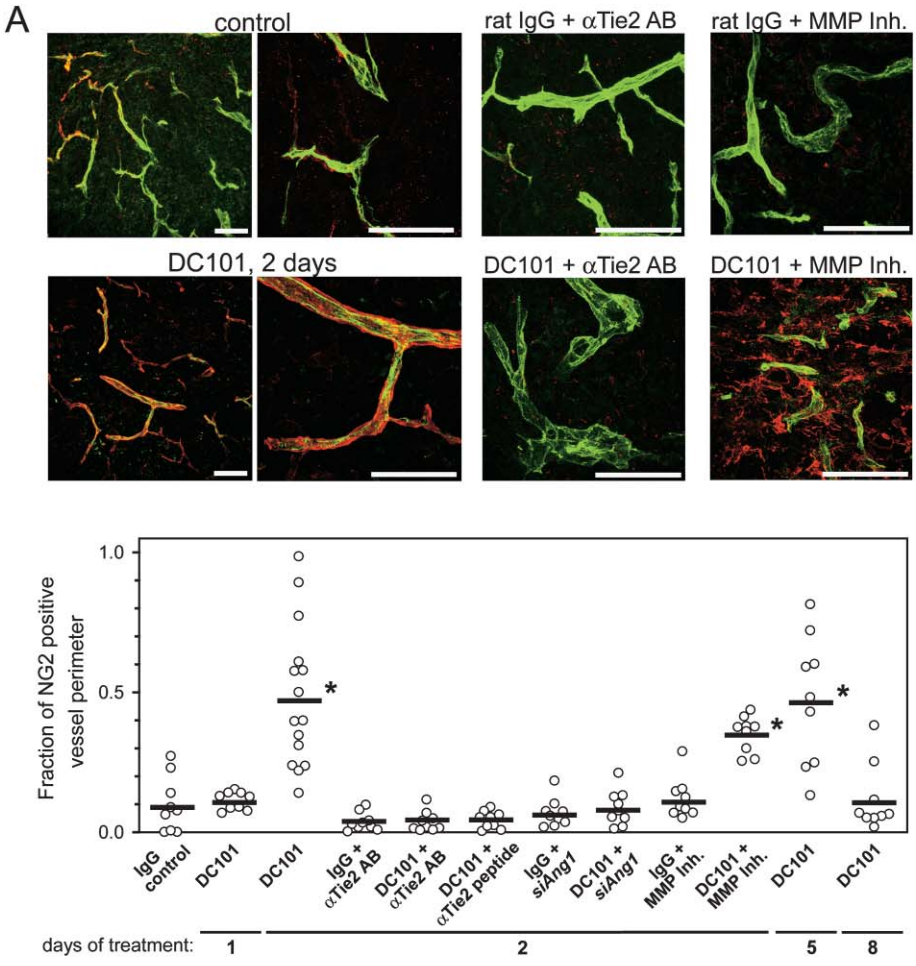

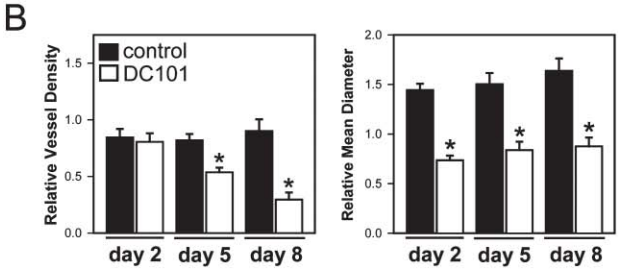

Figure 2. VEGFR2 blockade temporarily increases pericyte coverage of nonregressed tumor vessels via Tie2 activation

A: The number of pericytes (NG2 staining, red) closely associated with perfused tumor vessels (green) increased 2 and 5 days after initiation of DC101 treatment, compared to tumors treated with nonspecific control-IgG. This effect was not yet detectable on day 1 and was diminished by day 8. Blockade of Tie2 activation by an anti-Tie2 antibody (αTie2 AB), a Tie2-inhibiting peptide (αTie2 peptide), or downregulation of angiopoietin-1 expression in U87 tumor cells by siRNA technique (*siAng-1*) completely abolished the DC101-induced increase in pericyte coverage after 2 days. In contrast, matrix metalloproteinase (MMP) inhibition by GM6001 did not significantly decrease pericyte recruitment by DC101, but increased the number of additional, detached pericytes.

B: DC101 treatment reduced the diameter of enlarged tumor vessels, starting at day 2 of therapy. In contrast, vessel length density was not changed at day 2, but decreased progressively at later time points. Angiograms were obtained using dynamic multiphoton laser scanning microscopy in vivo (see Supplemental Figure S1 at http://www.cancercell.org/cgi/content/6/6/553/DC1/ for representative images and values). Scale bars, 100 μm. *$p < 0.05$, compared to rat-IgG treated control (2 days of treatment).

increase is due to the preferential pruning of pericyte-poor vessels (Benjamin et al., 1999), but if this were the case, the increased coverage should be accompanied by a decrease in vessel length per unit volume of tumor tissue; this was not observed in our study. Two days after the initial DC101 injection, when pericyte coverage reached its peak, we found a significant decrease in the diameter of tumor vessels, consistent with our previous data (Yuan et al., 1996; Kadambi et al., 2001; Tong et al., 2004), but there was no decrease in vessel length density in the treated mice compared to untreated controls or nonspecific IgG-treated controls (Figures 2A and 2B). Furthermore, by day 8, extensive vascular regression had occurred (Figure 2B and Supplemental Figure S1 at http://www.cancercell.org/cgi/content/full/6/6/553/DC1/), but pericyte coverage had fallen to the control level (Figure 2A), suggesting that the pericyte-covered vessels enjoyed no long-term survival advantage. These results suggest that, rather than selectively pruning pericyte-poor vessels, VEGFR2 blockade temporarily facilitates the recruitment of pericytes to tumor vessels.

Angiopoietin-1 upregulation in the tumor cells promotes pericyte recruitment to tumor vessels after VEGFR2 blockade

To investigate the molecular mechanisms of pericyte recruitment by VEGFR2 blockade, we used a cDNA microarray to examine the expression of 96 human and murine genes associated with angiogenesis and vessel maturation. At the time of peak pericyte coverage (day 2 after DC101 therapy), only two molecules were differentially regulated more than 3-fold: human angiopoietin-1 (Ang-1; 4.8-fold upregulation) and human Ephrin B2 (3.8-fold upregulation). Quantitative real-time PCR using species-specific primers confirmed only a nearly 3-fold increase in human Ang-1 transcripts at day 2, but not at day 8 (Table 2). Furthermore, increased synthesis of Ang-1 mRNA by cancer cells resulted in increased deposition of Ang-1 protein in proximity to its receptor Tie2 on endothelial cells at days 2 and 5, but, again, not at day 1 or day 8 (Figure 3A). Ang-1 upregulation at day 5 of DC101 therapy was also confirmed by Western blot analysis of whole tumor lysates (Figure 3B). An effect of VEGF/VEGFR2 signaling on the Ang-1/Tie2 pathway has not previously been shown.

Because Ang-1 is known to be involved in pericyte recruitment (Stoeltzing et al., 2003; Jain, 2003), our results suggest that Ang-1 mediates the DC101-induced recruitment of pericytes to tumor vessels. In order to confirm the causal role of Ang-1, we first used a Tie2-blocking antibody or peptide to block Ang-1/Tie2 signaling. In the presence of Tie2 blockade, DC101 failed to increase vascular pericyte coverage, consistent with our hypothesis (Figure 2A). DC101 therapy also failed to decrease mean vascular diameter (Figure 3C) when Tie-2 was blocked. A second experiment confirmed that *tumor cell*-derived Ang-1 is indeed responsible for pericyte recruitment after VEGFR2 blockade: when U87 glioma cells were stably transfected with Ang-1 siRNA (*siAng-1*), these cells expressed ~50% less Ang-1 mRNA in vitro and ~90% less Ang-1 protein near blood vessels in vivo (Figure 3A). In *siAng-1* tumors, DC101 therapy increased vascular Ang-1 protein deposition insufficiently: only levels similar to those in wild-type control tumors were reached (Figure 3A). Consequently, *siAng-1* tumors revealed a greatly reduced pericyte recruitment to tumor vessels at day 2 of DC101 therapy (Figure 2A). Collectively, these data suggest that pericyte re-

Table 2. Cancer cell-derived Ang-1 is differentially upregulated 2 days after DC101 treatment

	hAng-1	mAng-2	hAng-1/mAng-2	hEphrin B2	mEndoglin (CD105)	mEphrin B2	mEphB4	hPDGFB	mPDGFRβ	Coll IV
Controls	0.54 ± 0.14	2.55 ± 0.78	0.54 ± 0.20	0.33 ± 0.08	1.28 ± 0.14	1.33 ± 0.13	1.92 ± 0.22	0.24 ± 0.06	1.33 ± 0.13	1.54 ± 0.25
DC101 treated, day 2	1.44 ± 0.36*	1.07 ± 0.29	2.56 ± 0.74*	0.43 ± 0.11	1.37 ± 0.35	0.95 ± 0.14	1.45 ± 0.12	0.44 ± 0.19	1.13 ± 0.19	0.82 ± 0.18*
DC101 treated, day 8	0.21 ± 0.06^{+}	2.29 ± 0.14^{+}	0.10 ± 0.02^{+}	0.20 ± 0.02	1.66 ± 0.13	1.04 ± 0.12	2.67 ± 0.10^{+}	0.27 ± 0.08	2.69 ± 0.31^{+}	1.58 ± 0.09^{+}

Quantitative real-time PCR analysis of human and murine genes involved in vessel maturation and basement membrane synthesis. Tumors were dissected from controls (n = 8), 2 days after DC101 treatment (n = 8), or 8 days after DC101 treatment (n = 3). Four candidate genes were chosen based on the results of cDNA microarray analysis: hAng-1 was upregulated 4.8-fold and hEphrin B2 3.8-fold, while mCD105 was downregulated 2.5-fold and mEphrin B2 2.6-fold. In addition, we analyzed additional genes, known to be involved in vascular maturation, that were below the detection limit of the cDNA microarray: human PDGF-B, mouse PDGFRβ, and mouse EphB4. The ratio of hAng-1 to mAng-2 was determined separately for each animal, and means are given for each group. Values represent relative gene expression normalized to β-actin. *$p < 0.05$, compared to controls; $^{+}p < 0.05$, compared to DC101 treated, day 2. m, murine; h, human.

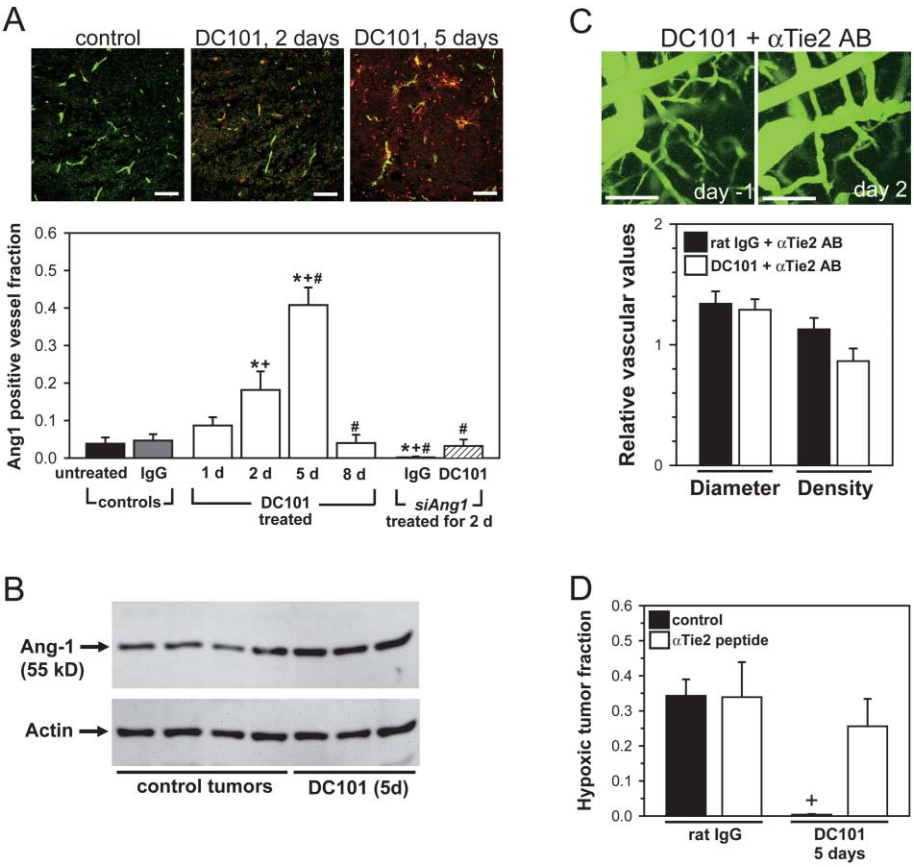

Figure 3. Angiopoietin-1 protein level increases after VEGFR2 blockade, which decreases the diameter of tumor vessels and induces tumor reoxygenation via Tie2 activation

A: Ang-1 protein (red) colocalized with perfused vessels (green) 2 and 5 days after initiation of DC101 therapy. In contrast, low levels of Ang-1 near perfused vessels was observed in control tumors, at day 1 and at day 8 after initiation of DC101 therapy, and when Ang-1 protein production was blocked in tumor cells by siRNA transfection (*siAng-1*).

B: Western blot analysis confirmed increased Ang-1 expression in whole tumor lysates at day 5.

C: Treatment with an anti-Tie2 antibody (αTie2 AB) inhibited the DC101-induced decrease in mean vessel diameter after 2 days.

D: Tie2 inhibition with an αTie2 peptide also diminished tumor reoxygenation at day 5 of DC101 therapy.

Scale bars, 100 μm. *$p < 0.05$, compared to untreated control; $^{+}p < 0.05$, compared to rat-IgG-treated control (day 2); #$p < 0.05$, compared to day 2 after initiation of DC101 therapy.

cruitment by tumor cell-derived Ang-1 plays a critical role in the normalization of vessel diameter after VEGFR2 blockade.

Ang-1 is also known to reduce vascular permeability of the blood-brain barrier (Lee et al., 2003). However, although we found that vascular permeability to albumin was reduced throughout the entire course of DC101 treatment (Supplemental Figure S1F), this reduction was independent of the kinetics of Ang-1 expression or pericyte coverage, which suggests that it was not mediated by Ang-1 exclusively.

We finally sought to demonstrate that vascular stabilization induced by angiopoietin-1 indeed results in better tumor oxygenation after VEGFR2 blockade. When the Tie2 receptor was blocked, reduction in tumor hypoxia at day 5 was diminished after DC101 therapy (Figure 3D), indicating a causal link between Ang-1-mediated vascular normalization and vascular function.

The abnormally thick basement membrane of brain tumor vessels is reduced during the normalization window

We also observed dramatic changes in the vascular basement membrane (BM) 2 to 5 days after DC101 injection. Whereas vessels in control tumors had an aberrantly thick, multilayer BM (as indicated by collagen IV staining), DC101 treatment reduced BM thickness on days 2 and 5, and (to a lesser degree) on day 8, but not on day 1 (Figure 4A). Similar changes occurred in the other major BM components (laminin, entactin, perlecan). The BM is shared by endothelial cells and pericytes and is a major component of the vascular wall. BM thickening has been reported in other tumor models (Baluk et al., 2003), and has also been observed in diabetes mellitus and neurodegenerative diseases, where it was linked to impaired vascular function (Tsilibary, 2003; Farkas et al., 2000). In addition, BM thickening is seen in human glioblastoma multiforme: a majority (18 out of 30) of glioblastoma patients show tumor vessels characterized by a pathologically thick BM (Figure 4B).

VEGFR2 blockade degrades basement membrane via activation of matrix metalloproteinases

Because Tie-2 blockade did not affect the thinning of tumor vessel BM, indicating that increased pericyte involvement was not responsible (Figure 5A), we investigated the possibility that reduced production and/or increased degradation of BM components was responsible for the change in BM morphology. Indeed, the mRNA expression of murine collagen IV was reduced after DC101 treatment (Table 2). However, increased activity of the matrix metalloproteinases (MMPs) -2 and -9, which can rapidly degrade collagen IV and other components of the BM, may be functionally more important. In contrast, MMP-9 was shown to be downregulated by inhibition of VEGFR2 (Sweeney et al., 2002) or VEGFR1 (Hiratsuka et al., 2002) signaling in murine lung endothelial cells in vivo and in vitro. In U87 gliomas, we found that MMP-2 and -9 proteins were expressed around vessels at equivalent levels in control and treated animals (not shown), so we investigated whether posttranslational MMP activation occurs after VEGFR2 blockade. Surprisingly, using in situ zymography, we discovered an

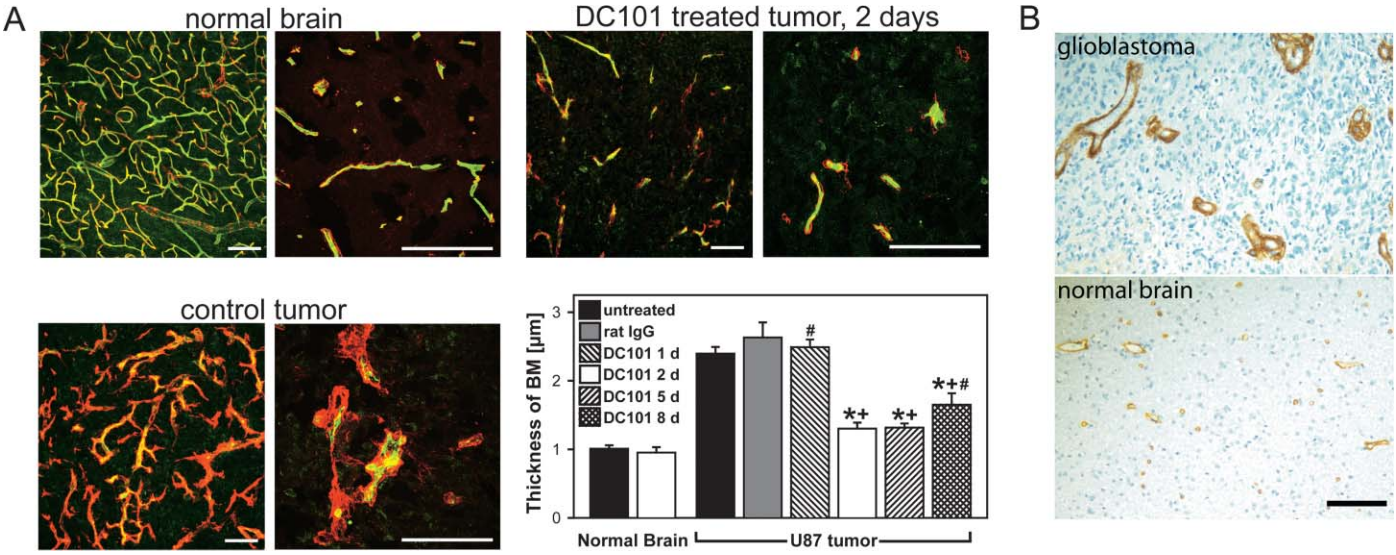

Figure 4. VEGFR2 blockade thins the abnormally thick basement membrane (BM) of tumor vessels

A: The vascular basement membrane (collagen IV staining, red) was thin and closely associated with perfused vessels (green) in normal brain, but appeared thickened, disorganized, and occasionally multilayered in control tumors. DC101 reduced the mean basement membrane thickness at day 2 and 5. This effect was not visible before day 2, and was diminished by day 8 of DC101 therapy. *$p < 0.05$, compared to untreated control; $^{+}p < 0.05$, compared to control treated with rat nonspecific IgG (day 2); #$p < 0.05$, compared to day 2 after initiation of DC101 therapy.
B: A majority (18/30) of glioblastoma patients showed tumor vessels with a thickened basement membrane.
Scale bars, 100 μm.

increase in collagenase IV activity at the vascular wall 2 days after DC101 therapy (Figure 5B). Furthermore, coadministration of a broad-spectrum inhibitor of the matrix metalloproteinases (MMPs), GM6001, completely abolished the DC101-induced BM thinning (Figure 5C).

Discussion

Collectively, these results demonstrate that VEGFR2 blockade can temporarily normalize tumor vessel structure (pericyte and basement membrane coverage), leading to improved vascular function (tumor oxygenation) and enhanced response to radiation therapy. Figure 6A illustrates the time course of these changes, while the proposed underlying molecular mechanisms are summarized in Figure 6B.

Our findings suggest several important changes to the existing paradigm. Contrary to the view that the primary result of anti-VEGF treatment is to prune tumor vessels that are devoid of pericytes (Benjamin et al., 1999), we show that, during the normalization window in brain tumors, VEGFR2 blockade temporarily recruits pericytes to blood vessels by activating Ang-1/Tie2 signaling. These fortified vessels become more efficient, enhancing oxygen delivery to the tumor.

Ang-1 has been implicated in facilitating interaction between endothelial cells and pericytes during angiogenesis (Jain, 2003). Others have shown that expression of Ang-1 is restricted to cancer cells in human glioblastoma multiforme (Stratmann et al., 1998) and glioma animal models (Holash et al., 1999). Our results extend this finding, showing that Ang-1 protein produced by tumor cells is found mainly in the vicinity of vessels, where it is sequestered by its endothelial receptor Tie2. Ang-1 has well-defined, substantial effects on the vasculature (Jain and Munn, 2000): it has been shown to increase pericyte coverage, and several studies indicate that this process implies vessel maturation and improved vascular function (Hawighorst et al., 2002; Stoeltzing et al., 2003). Furthermore, even in the complete absence of mural cells, recombinant Ang-1 can restore a hierarchical vasculature and inhibit retinal edema and hemorrhage (Uemura et al., 2002). It also reduces vascular permeability in the skin (Thurston et al., 1999), tumors (Stoeltzing et al., 2003), and an in vitro blood-brain barrier model by maturation of endothelial cells (Lee et al., 2003). Consistent with these findings, the increased expression of the naturally occurring Ang-1 antagonist, Ang-2, in glioma vessels is associated with their destabilization (Holash et al., 1999) and is negatively correlated with pericyte coverage, both in human glioblastoma specimens (Stratmann et al., 1998) and experimental gliomas (Koga et al., 2001). Here we show that an increase in the Ang-1/Ang-2 ratio with activated Ang-1/Tie2 signaling after VEGFR2 blockade recruits pericytes to tumor vessels and subsequently reduces their enlarged diameter, demonstrating a profound effect of this phenomenon on the tumor vessel network. Therefore, Ang-1 upregulation acts synergistically with the direct effects of VEGFR2 blockade on endothelial cells to normalize brain tumor vessels.

Ang-1 upregulation after VEGFR2 blockade is not specific for brain tumor vessels: in subcutaneously growing MCaIV mammary carcinomas, DC101 therapy likewise resulted in increased expression of Ang-1 and its vascular deposition (Supplemental Figure S2) at a time of increased pericyte coverage (Tong et al., 2004). However, neither Ang-1 expression nor pericyte coverage was changed in normal vessels of the brain, heart, and kidney during DC101 therapy (unpublished data), indicating that Ang-1 upregulation after VEGFR2 blockade is specific for the tumor environment.

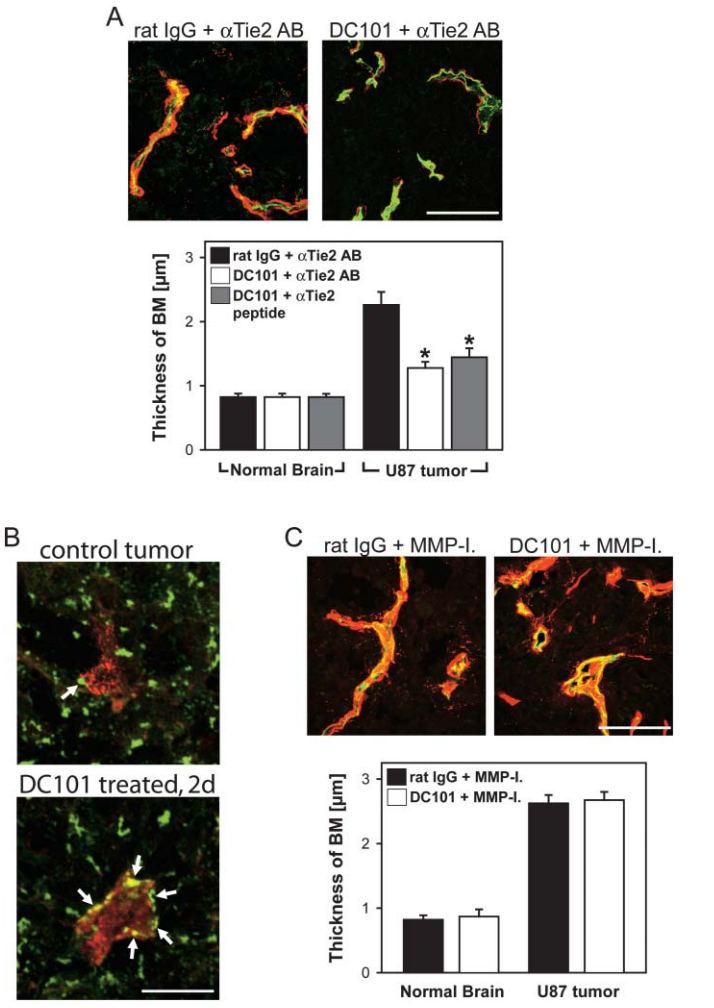

Figure 5. Basement membrane thinning after VEGFR2 blockade results from increased degradation by matrix metalloproteinases

A: Interference with Tie-2 signaling did not affect basement membrane normalization 2 days after initiation of DC101 therapy.
B: Perfused vessels (red) revealed an increase in collagenase IV activity (green) near the vascular wall (arrows) at day 2 of DC101 therapy, compared to control tumors. Extravascular collagenase IV activity was similar in both groups.
C: GM6001, a broad-spectrum MMP inhibitor, completely abolished the decrease of BM thickness induced by DC101.
Scale bars, 100 μm (**A** and **C**), 20 μm (**B**).
*$p < 0.05$, compared to control treated with rat nonspecific IgG plus αTie2 antibody (day 2).

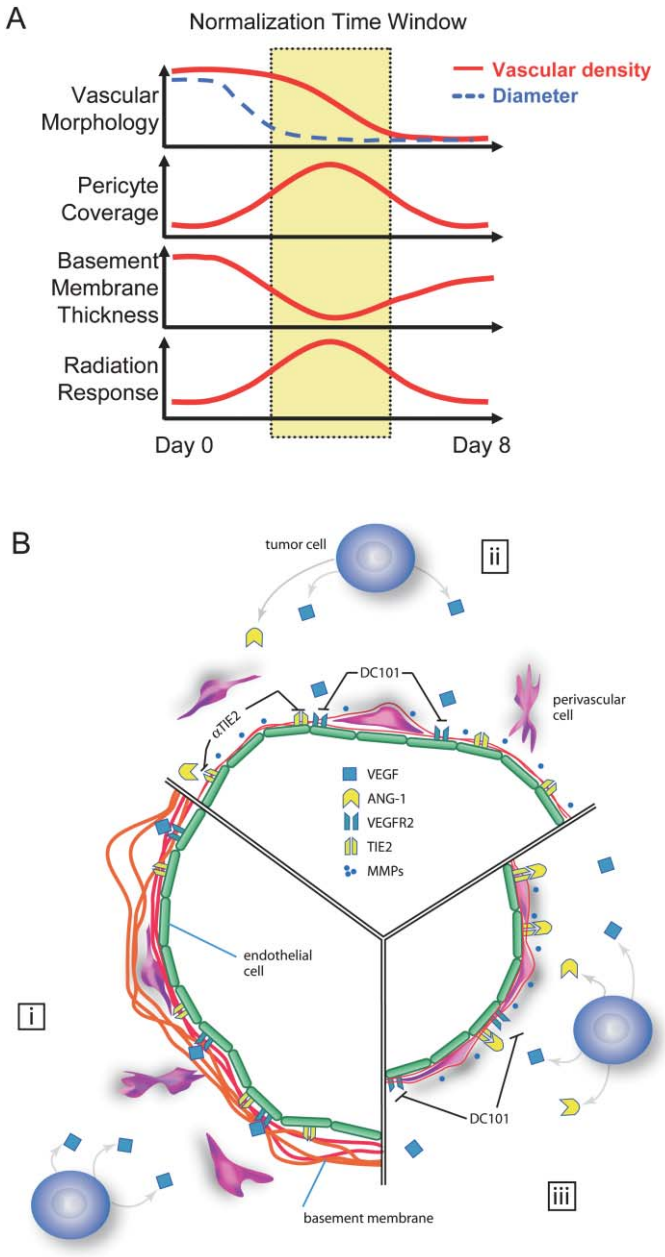

Figure 6. Time course and mechanisms of vascular normalization, illustrated in schematic diagrams

A: VEGFR2 blockade produces a time window of morphological and functional normalization of tumor vessels, which determines the tumor response to radiotherapy.
B: Mechanisms of tumor vessel normalization by DC101. (i) Control tumors are characterized by tortuous, dilated blood vessels that lack tight pericyte coverage and display a thickened, detached basement membrane. These vascular abnormalities occur in the presence of excessive VEGF/VEGFR2 signaling. (ii) Within two days, VEGFR2 blockade can normalize BM morphology by activation of matrix metalloproteinases, increasing BM degradation. However, when Tie2 signaling is not activated, VEGFR2 blockade fails to improve other vascular abnormalities. This occurs when Tie2 is pharmacologically inhibited (left), or when Ang-1 expression is low, as it is in *siAng-1*-transfected tumors, or on day 8 of therapy (right). (iii) After VEGFR2 blockade, the upregulation of Ang-1 in cancer cells and its binding to Tie2 are required for full vascular normalization.

It has previously been shown that chronic overexpression of angiopoietin-1 starting during embryonic development increases the diameter of normal vessels (Thurston et al., 1999, 2000), while transient Ang-1 overexpression in normal adult vasculature (Thurston et al., 2000) or chronic Ang-1 overexpression in tumors (Hawighorst et al., 2002) does not significantly change the vessel diameter. We show that transient Ang-1 overexpression can reduce the vascular diameter of tumor vessels.

The mechanism by which Ang-1 is upregulated after VEGFR2 inhibition remains unknown. Ang-1 protein (as detected by Western blot) was not changed in U87 cells in vitro after exposure to DC101, which makes a direct effect of DC101

on the tumor cells unlikely. Likewise, even though Ang-1 expression was increased after reoxygenation of cultured astrocytes (Song et al., 2002), we could not confirm a change in Ang-1 protein in U87 glioma cells after 24 hr of hypoxia (0.5% oxygen) and at different time points of reoxygenation (data not shown). We would therefore rather hypothesize that a paracrine mediator that binds to adjacent tumor cells is produced by endothelial cells after VEGFR2 blockade, which, in turn, increases their Ang-1 synthesis.

Our study provides evidence that severe abnormalities of the vascular basement membrane in glioma vessels are mediated by VEGF signaling, since VEGFR2 blockade restores a thinner, more closely attached BM monolayer by increasing collagen IV degradation by MMPs. The thick, disorganized basement membrane in untreated tumors likely contributes to impaired vascular function. It is plausible that a thickened sheet of extracellular matrix can affect the extravasation of oxygen, drugs, and nutrients (Tsilibary, 2003; Farkas et al., 2000). In contrast, subcutaneously implanted mammary carcinomas have incomplete vascular BM coverage. In these tumors, VEGFR2 blockade increases BM coverage to near normal levels (Tong et al., 2004). These seemingly contradictory findings illustrate that the phenotype of the tumor vessel BM is dependent on the local microenvironment. In both cases, VEGFR2 blockade appears to alter BM homeostasis, shifting the rates of BM synthesis and degradation to produce a more normal BM phenotype. Our study not only sheds light on the mechanism of BM thickening in gliomas but also demonstrates that it can be normalized by disrupting the VEGF pathway.

Most importantly, our results alleviate the concern that, by destroying blood vessels, antiangiogenic therapy will invariably increase tumor hypoxia, leading to an increased resistance to radiation and increased metastatic potential (Bottaro and Liotta, 2003). On the contrary, we show that a properly timed VEGFR2 blockade can transiently decrease hypoxia, opening up a window of opportunity to irradiate tumors more effectively.

In fact, in our experiments, tumor oxygen status was the main factor determining the efficacy of radiation. The recent study by Garcia-Barros et al. (2003) suggested that damage to tumor-associated endothelial cells plays a crucial role in the outcome of radiation therapy. By blocking the main receptor for VEGF, a survival factor for tumor endothelial cells, DC101 may enhance the damaging effect of radiation to tumor vessels (Dvorak, 2002; Ferrara et al., 2004; Kerbel and Folkman, 2002). However, the impact of this DC101-induced effect was not dramatic and seemed to be independent of that caused by radiation, as the tumor growth delay induced by DC101 was virtually identical when the antibody was used alone or in combination with nonoptimal radiation schedules (RT1, RT2, RT3, RT5) compared to untreated controls or radiation monotherapy, respectively. Only when DC101 minimized tissue hypoxia during RT4 did the combined effect become synergistic—that is, significantly greater than additive. In contrast, DC101-induced apoptosis of tumor and vascular cells was similar on day 5 (corresponding to RT4) and on day 8 (corresponding to RT5); therefore, it did not coincide with the synergistic effect of combination therapy that was exclusively observed for RT4. Interestingly enough, based on the literature (Kwak et al., 2000; Cho et al., 2004), one could argue that overexpression of Ang-1 per se during the normalization period should have decreased rather than increased the sensitivity of endothelial cells to radiation. Improved oxygenation significantly overcompensated for this assumed radioprotection of endothelial cells by Ang-1, emphasizing once again that oxygen status dominates other factors in determining the outcome of optimally combined therapy.

The therapeutic gain achieved due to DC101 in the synergistic combination group RT4 is substantial—from a tumor growth delay of 12.5 days for radiation alone to 21.7 days for DC101+RT4. To achieve a 21.7-day growth delay with radiation alone, we would need to increase its total dose from 21 to 35–38 Gy (Kozin et al., 2001). The fact that we saw such a substantial increase in growth delay attests to the importance of tumor oxygenation for radiation therapy (Hall, 2000).

The ability to measure tumor hypoxia in patients using noninvasive imaging techniques may enable clinicians to optimize the combination of anti-VEGF treatment with radiation therapy. Similar optimization strategies may also improve response to chemotherapy. It is tempting to speculate that, if the time course of vascular changes induced by VEGF blockade is taken into account, one might achieve a survival advantage greater than the 5 months seen in the recent landmark clinical trial of combination therapy (Hurwitz et al., 2004).

Experimental procedures

Animal model and cell lines

We implanted cranial windows into 8- to 10-week-old male nude mice as previously described (Yuan et al., 1994). After one week, we implanted small (0.2–0.3 mm diameter) fragments of U87 glioma tumors superficially into the cerebral cortex under the cranial window at a depth of approximately 0.4 mm. Animals were anesthetized with ketamine/xylazine (100/10 mg/kg, i.m.) for all experimental procedures. Intravenous injections were performed using a lateral tail vein. All cell lines were maintained in DMEM medium with 10% FBS. To obtain a stable short interfering hairpin RNA (siRNA) construct for silencing the angiopoietin-1 gene (*siAng-1*), we used oligos 5′-GAT CCG GAA GAG TTG GAC ACC TTA TTC AAG AGA TAA GGT GTC CAA CTC TTC CTT TTT TGG AAA-3′ and 5′-AGC TTT TCC AAA AAA GGA AGA GTT GGA CAC CTT ATC TCT TGA ATA AGG TGT CCA ACT CTT CCG-3′ and subcloned the product into a pSilencer 3.1-H1 hygro plasmid (Ambion). The pSilencer vector was stably transfected into U87 cells using Lipofectamine 2000 (Invitrogen), and transfected cells were selected with hygromycin. All mouse experiments were approved by the Massachusetts General Hospital Subcommittee on Research Animal Care.

Treatment protocol

For combination therapy, U87 gliomas constitutively expressing GFP were monitored by intravital fluorescence microscopy. When grown to a diameter of 2–2.5 mm (defined as day 0), treatment was started with either the monoclonal VEGFR2-specific antibody DC101 (rat anti-mouse; ImClone Systems Inc.) or fractionated radiation. DC101 was injected i.p. at a dose of 40 mg/kg every 3 days, for a total of 3 injections. γ radiation was given locally to the upper part of the brain in 3 daily fractions, 7 Gy each, at a dose rate of 4.6 Gy/min. When the treatment modalities were combined, radiotherapy was started at one of 5 different time points relative to the first DC101 injection: 9 or 2 days before (R1 and R2 in Figure 1A, respectively), or 1, 4, or 7 days after (R3, R4, and R5, respectively). Therapeutic efficacy was evaluated by measuring tumor growth delay (versus untreated control), as defined by the time taken for tumors to double their initial diameter. Groups consisted of 7–8 animals.

For all other studies, mice bearing U87 gliomas were injected with DC101 or nonspecific rat IgG control antibody (Jackson ImmunoResearch) i.p. at a dose of 40 mg/kg every third day for a maximum of three doses (days 0, 3, and 6). An additional control group with size-matched tumors received no specific treatment. When tumors were collected for histological analyses, treatment was scheduled to assure same tumor sizes (3–4 mm) at the time of sacrifice. To block angiopoietin-1/Tie2 receptor signaling, animals were injected either with 20 mg/kg anti-mouse Tie2 blocking antibody i.p. (R&D Systems) or with 125 nmol of the Tie2 blocking peptide

NLLMAAS (Tournaire et al., 2004) stereotactically into the tumor. For inhibition of MMPs, mice were injected i.p. with 150 μg of the broad spectrum MMP inhibitor GM 6001 (Ryss Lab). All agents were given 30 min after the mice received either DC101 or nonspecific rat IgG control antibody, and the animals were sacrificed 2 or 5 days later.

Angiography by multiphoton laser scanning microscopy (MPLSM) and microvascular permeability measurement

In vivo MPLSM angiography of glioblastoma vessels was performed after i.v. injection of 0.1 ml 10 mg/ml FITC-Dextran (2M MW, Sigma) as described previously (Brown et al., 2001). For each tumor, four adjacent images representing tumor vessels −75 to −200 μm below the brain surface were obtained through the cranial window at day −1, and the same regions identified by using landmarks of the overlaying pial vasculature were recorded at days 1, 2, 5, and/or 8 (n = 4 animals per group). Vessel length density, diameter, and volume were calculated for each vessel using NIH IMAGE 1.63 software (http://rsb.info.nih.gov/nih-image/), and means are expressed relative to the value that was obtained in the same tumor region one day before initiation of treatment. The microvascular permeability to albumin was measured as previously described (Yuan et al., 1996).

Histology and immunostaining

Tumor-bearing mice were injected i.v. with biotinylated lectin (Vector Laboratories), heart-perfused with 4% paraformaldehyde, and blood vessels were stained with a Streptavidin-conjugated fluorochrome (Alexa 488 or Alexa 647; Molecular Probes). Thin (10 μm) or thick (100 μm) sections were incubated at 4°C overnight with one of the following antibodies: rabbit anti-collagen IV (1:2000; Chemicon), rabbit anti-NG2 (1:1000; Chemicon), or goat anti-Ang-1 (1:100; Santa Cruz), and subsequently with Cy3-conjugated secondary antibodies (1:200, Jackson ImmunoResearch). Apoptosis staining was performed by the indirect TUNEL method using the ApopTag Red In Situ Apoptosis Detection Kit (Chemicon) according to manufacturers' instructions. To detect tumor hypoxia, 60 mg/kg pimonidazole was injected i.v. 1 hr before brains were rapidly frozen at −80°C. The Hypoxyprobe-1 Kit (Chemicon) was used to detect pimonidazole-protein adducts in 2 brain regions per animal spaced 200 μm apart (n = 3 to 4 animals per group). Pericyte coverage was quantified by calculating the fraction of vessel perimeter that overlapped with NG2 staining. For this purpose, confocal image stacks (60 μm) of three well-vascularized tumor regions were obtained, maximum intensity projections were generated, and calculations were performed by a macro within NIH IMAGE (n = 3 to 5 animals per group). A similar method was used to calculate colocalization of Ang-1 with perfused vessels. To determine the average thickness of the basement membrane as indicated by collagen IV staining, 4 × 4 grids were superimposed on three 432 × 330 μm high-resolution images from 10 μm thick sections using Adobe Photoshop software (n = 3 to 4 animals per group). Wherever grid lines intersected collagen IV-positive basement membrane structures, their diameter and smallest distance to the lectin signal was measured.

In situ zymography was performed after the lectin staining of perfused vessels by overnight incubation of unfixed frozen sections with DQ collagen IV (Molecular Probes), which contains quenched fluorescence that is released after collagen IV degradation.

To detect basement membrane structures in human brain tumors, a tissue microarray containing 30 cases of histologically confirmed glioblastomas (2 samples per patient, Petagen) and 2 normal brain samples was stained with a rabbit anti-collagen IV antibody and the Envision detection kit (both DAKO). Basement membrane thickness of tumor vessels was scored by an independent observer in comparison to normal brain (thicker/normal/thinner).

Expression of genes involved in angiogenesis and vessel maturation

Total RNA was extracted from tumors of 3 mm diameter using TRIzol Reagent (Invitrogen). To screen for relative differential expression of multiple genes, cDNA arrays containing 96 genes involved in angiogenesis and vessel maturation were used according to manufacturer's instructions (GEArray Q Series). Chemiluminescent spots were quantified by densitometry and normalized with β-actin (FluoroChem 8800 system). A change of more than 3-fold between controls and treated tumors was considered significant differential expression; a change of 2- to 3-fold was regarded as marginal. Using real-time PCR, we quantified mRNA levels of various candidate molecules that were identified by cDNA array analysis. Lux fluorogenic primers (Invitrogen) specific for the mouse or human isoform of each mRNA species were designed using Lux Online Primer Software (Invitrogen; primer sequences available on request). Quantitative RT-PCRs were performed on the ABI 7700 sequence detection system (Applied Biosystems). All experiments were performed in duplicate, and a standard curve for the specific cDNA of interest was run with every PCR reaction; amounts of cDNA are expressed relative to this standard curve. Final quantification of each cDNA sample was relative to human or mouse β-actin according to the manufacturer's instructions (Applied Biosystems).

Ang-1 protein expression was determined by Western blot analysis. Total protein from tumor xenografts was extracted in RIPA buffer, and 30 μg of protein was separated on a 10% SDS-PAGE gel, transferred to PVDF membrane, and incubated with anti-Ang1 antibody (1:1000, 4°C overnight). Ang1 was visualized using the enhanced chemiluminescence kit (Amersham).

Statistical analysis

Data are expressed as mean ± SEM. The principal statistical test was the Student's t test (two tailed). $p < 0.05$ was considered to be statistically significant.

Acknowledgments

Supported by the Goldhirsh Foundation and the National Cancer Institute. F.W. is a fellow of the Deutsche Forschungsgemeinschaft, Emmy-Noether Programm. We thank Sylvie Roberge for her excellent technical assistance, and Yves Boucher, Dan Duda, Tim Padera, and Herman D. Suit for helpful comments on the manuscript. The monoclonal antibody DC101 was generated by ImClone Systems, of which D.J.H. is an employee. The remaining authors have no financial interest related to this work.

Received: July 29, 2004
Revised: September 29, 2004
Accepted: October 13, 2004
Published: December 20, 2004

References

Baluk, P., Morikawa, S., Haskell, A., Mancuso, M., and McDonald, D.M. (2003). Abnormalities of basement membrane on blood vessels and endothelial sprouts in tumors. Am. J. Pathol. *163*, 1801–1815.

Benjamin, L.E., Golijanin, D., Itin, A., Pode, D., and Keshet, E. (1999). Selective ablation of immature blood vessels in established human tumors follows vascular endothelial growth factor withdrawal. J. Clin. Invest. *103*, 159–165.

Bottaro, D.P., and Liotta, L.A. (2003). Cancer: Out of air is not out of action. Nature *423*, 593–595.

Brown, E.B., Campbell, R.B., Tsuzuki, Y., Xu, L., Carmeliet, P., Fukumura, D., and Jain, R.K. (2001). In vivo measurement of gene expression, angiogenesis and physiological function in tumors using multiphoton laser scanning microscopy. Nat. Med. *7*, 864–868.

Carmeliet, P., and Jain, R.K. (2000). Angiogenesis in cancer and other diseases. Nature *407*, 249–257.

Cho, C.H., Kammerer, R.A., Lee, H.J., Yasunaga, K., Kim, K.T., Choi, H.H., Kim, W., Kim, S.H., Park, S.K., Lee, G.M., and Koh, G.Y. (2004). Designed angiopoietin-1 variant, COMP-Ang1, protects against radiation-induced endothelial cell apoptosis. Proc. Natl. Acad. Sci. USA *101*, 5553–5558.

Dvorak, H.F. (2002). Vascular permeability factor/vascular endothelial growth factor: A critical cytokine in tumor angiogenesis and a potential target for diagnosis and therapy. J. Clin. Oncol. *20*, 4368–4380.

Farkas, E., De Jong, G.I., de Vos, R.A., Jansen Steur, E.N., and Luiten, P.G. (2000). Pathological features of cerebral cortical capillaries are doubled in Alzheimer's disease and Parkinson's disease. Acta Neuropathol. (Berl.) *100*, 395–402.

Ferrara, N., Hillan, K.J., Gerber, H.P., and Novotny, W. (2004). Discovery and development of bevacizumab, an anti-VEGF antibody for treating cancer. Nat. Rev. Drug Discov. *3*, 391–400.

Garcia-Barros, M., Paris, F., Cordon-Cardo, C., Lyden, D., Rafii, S., Haimovitz-Friedman, A., Fuks, Z., and Kolesnick, R. (2003). Tumor response to radiotherapy regulated by endothelial cell apoptosis. Science *300*, 1155–1159.

Gorski, D.H., Mauceri, H.J., Salloum, R.M., Gately, S., Hellman, S., Beckett, M.A., Sukhatme, V.P., Soff, G.A., Kufe, D.W., and Weichselbaum, R.R. (1998). Potentiation of the antitumor effect of ionizing radiation by brief concomitant exposures to angiostatin. Cancer Res. *58*, 5686–5689.

Hall, E.J. (2000). The oxygen effect and reoxygenation. In Radiobiology for the Radiologist, E.J. Hall (Philadelphia: JB Lippincott), pp. 91–111.

Hawighorst, T., Skobe, M., Streit, M., Hong, Y.K., Velasco, P., Brown, L.F., Riccardi, L., Lange-Asschenfeldt, B., and Detmar, M. (2002). Activation of the tie2 receptor by angiopoietin-1 enhances tumor vessel maturation and impairs squamous cell carcinoma growth. Am. J. Pathol. *160*, 1381–1392.

Hiratsuka, S., Nakamura, K., Iwai, S., Murakami, M., Itoh, T., Kijima, H., Shipley, J.M., Senior, R.M., and Shibuya, M. (2002). MMP9 induction by vascular endothelial growth factor receptor-1 is involved in lung-specific metastasis. Cancer Cell *2*, 289–300.

Holash, J., Maisonpierre, P.C., Compton, D., Boland, P., Alexander, C.R., Zagzag, D., Yancopoulos, G.D., and Wiegand, S.J. (1999). Vessel cooption, regression, and growth in tumors mediated by angiopoietins and VEGF. Science *284*, 1994–1998.

Hurwitz, H., Fehrenbacher, L., Novotny, W., Cartwright, T., Hainsworth, J., Heim, W., Berlin, J., Baron, A., Griffing, S., Holmgren, E., et al. (2004). Bevacizumab plus irinotecan, fluorouracil, and leucovorin for metastatic colorectal cancer. N. Engl. J. Med. *350*, 2335–2342.

Inai, T., Mancuso, M., Hashizume, H., Baffert, F., Haskell, A., Baluk, P., Hu-Lowe, D.D., Shalinsky, D.R., Thurston, G., Yancopoulos, G.D., and McDonald, D.M. (2004). Inhibition of vascular endothelial growth factor (VEGF) signaling in cancer causes loss of endothelial fenestrations, regression of tumor vessels, and appearance of basement membrane ghosts. Am. J. Pathol. *165*, 35–52.

Jain, R.K. (2001). Normalizing tumor vasculature with anti-angiogenic therapy: A new paradigm for combination therapy. Nat. Med. *7*, 987–989.

Jain, R.K. (2003). Molecular regulation of vessel maturation. Nat. Med. *9*, 685–693.

Jain, R.K., and Munn, L.L. (2000). Leaky vessels? Call Ang1! Nat. Med. *6*, 131–132.

Kadambi, A., Mouta, C.C., Yun, C.O., Padera, T.P., Dolmans, D.E., Carmeliet, P., Fukumura, D., and Jain, R.K. (2001). Vascular endothelial growth factor (VEGF)-C differentially affects tumor vascular function and leukocyte recruitment: Role of VEGF-receptor 2 and host VEGF-A. Cancer Res. *61*, 2404–2408.

Kerbel, R., and Folkman, J. (2002). Clinical translation of angiogenesis inhibitors. Nat. Rev. Cancer *2*, 727–739.

Koga, K., Todaka, T., Morioka, M., Hamada, J., Kai, Y., Yano, S., Okamura, A., Takakura, N., Suda, T., and Ushio, Y. (2001). Expression of angiopoietin-2 in human glioma cells and its role for angiogenesis. Cancer Res. *61*, 6248–6254.

Kozin, S.V., Boucher, Y., Hicklin, D.J., Bohlen, P., Jain, R.K., and Suit, H.D. (2001). Vascular endothelial growth factor receptor-2-blocking antibody potentiates radiation-induced long-term control of human tumor xenografts. Cancer Res. *61*, 39–44.

Kwak, H.J., Lee, S.J., Lee, Y.H., Ryu, C.H., Koh, K.N., Choi, H.Y., and Koh, G.Y. (2000). Angiopoietin-1 inhibits irradiation- and mannitol-induced apoptosis in endothelial cells. Circulation *101*, 2317–2324.

Lee, C.G., Heijn, M., di Tomaso, E., Griffon-Etienne, G., Ancukiewicz, M., Koike, C., Park, K.R., Ferrara, N., Jain, R.K., Suit, H.D., and Boucher, Y. (2000). Anti-vascular endothelial growth factor treatment augments tumor radiation response under normoxic or hypoxic conditions. Cancer Res. *60*, 5565–5570.

Lee, S.W., Kim, W.J., Choi, Y.K., Song, H.S., Son, M.J., Gelman, I.H., Kim, Y.J., and Kim, K.W. (2003). SSeCKS regulates angiogenesis and tight junction formation in blood-brain barrier. Nat. Med. *9*, 900–906.

Ma, J., Pulfer, S., Li, S., Chu, J., Reed, K., and Gallo, J.M. (2001). Pharmacodynamic-mediated reduction of temozolomide tumor concentrations by the angiogenesis inhibitor TNP-470. Cancer Res. *61*, 5491–5498.

Mauceri, H.J., Hanna, N.N., Beckett, M.A., Gorski, D.H., Staba, M.J., Stellato, K.A., Bigelow, K., Heimann, R., Gately, S., Dhanabal, M., et al. (1998). Combined effects of angiostatin and ionizing radiation in antitumour therapy. Nature *394*, 287–291.

Millauer, B., Shawver, L.K., Plate, K.H., Risau, W., and Ullrich, A. (1994). Glioblastoma growth inhibited in vivo by a dominant-negative Flk-1 mutant. Nature *367*, 576–579.

Murata, R., Nishimura, Y., and Hiraoka, M. (1997). An antiangiogenic agent (TNP-470) inhibited reoxygenation during fractionated radiotherapy of murine mammary carcinoma. Int. J. Radiat. Oncol. Biol. Phys. *37*, 1107–1113.

Plate, K.H., Breier, G., Weich, H.A., and Risau, W. (1992). Vascular endothelial growth factor is a potential tumour angiogenesis factor in human gliomas in vivo. Nature *359*, 845–848.

Rampling, R., Cruickshank, G., Lewis, A.D., Fitzsimmons, S.A., and Workman, P. (1994). Direct measurement of pO2 distribution and bioreductive enzymes in human malignant brain tumors. Int. J. Radiat. Oncol. Biol. Phys. *29*, 427–431.

Rofstad, E.K., Henriksen, K., Galappathi, K., and Mathiesen, B. (2003). Antiangiogenic treatment with thrombospondin-1 enhances primary tumor radiation response and prevents growth of dormant pulmonary micrometastases after curative radiation therapy in human melanoma xenografts. Cancer Res. *63*, 4055–4061.

Song, H.S., Son, M.J., Lee, Y.M., Kim, W.J., Lee, S.W., Kim, C.W., and Kim, K.W. (2002). Oxygen tension regulates the maturation of the blood-brain barrier. Biochem. Biophys. Res. Commun. *290*, 325–331.

Stoeltzing, O., Ahmad, S.A., Liu, W., McCarty, M.F., Wey, J.S., Parikh, A.A., Fan, F., Reinmuth, N., Kawaguchi, M., Bucana, C.D., and Ellis, L.M. (2003). Angiopoietin-1 inhibits vascular permeability, angiogenesis, and growth of hepatic colon cancer tumors. Cancer Res. *63*, 3370–3377.

Stratmann, A., Risau, W., and Plate, K.H. (1998). Cell type-specific expression of angiopoietin-1 and angiopoietin-2 suggests a role in glioblastoma angiogenesis. Am. J. Pathol. *153*, 1459–1466.

Sweeney, P., Karashima, T., Kim, S.J., Kedar, D., Mian, B., Huang, S., Baker, C., Fan, Z., Hicklin, D.J., Pettaway, C.A., and Dinney, C.P. (2002). Antivascular endothelial growth factor receptor 2 antibody reduces tumorigenicity and metastasis in orthotopic prostate cancer xenografts via induction of endothelial cell apoptosis and reduction of endothelial cell matrix metalloproteinase type 9 production. Clin. Cancer Res. *8*, 2714–2724.

Teicher, B.A., Holden, S.A., Ara, G., Dupuis, N.P., Liu, F., Yuan, J., Ikebe, M., and Kakeji, Y. (1995). Influence of an anti-angiogenic treatment on 9L gliosarcoma: Oxygenation and response to cytotoxic therapy. Int. J. Cancer *61*, 732–737.

Thurston, G., Suri, C., Smith, K., McClain, J., Sato, T.N., Yancopoulos, G.D., and McDonald, D.M. (1999). Leakage-resistant blood vessels in mice transgenically overexpressing angiopoietin-1. Science *286*, 2511–2514.

Thurston, G., Rudge, J.S., Ioffe, E., Zhou, H., Ross, L., Croll, S.D., Glazer, N., Holash, J., McDonald, D.M., and Yancopoulos, G.D. (2000). Angiopoietin-1 protects the adult vasculature against plasma leakage. Nat. Med. *6*, 460–463.

Tong, R.T., Boucher, Y., Kozin, S.V., Winkler, F., Hicklin, D.J., and Jain, R.K. (2004). Vascular normalization by vascular endothelial growth factor receptor 2 blockade induces a pressure gradient across the vasculature and improves drug penetration in tumors. Cancer Res. *64*, 3731–3736.

Tournaire, R., Simon, M.P., le Noble, F., Eichmann, A., England, P., and Pouyssegur, J. (2004). A short synthetic peptide inhibits signal transduction, migration and angiogenesis mediated by Tie2 receptor. EMBO Rep. *5*, 262–267.

Tsilibary, E.C. (2003). Microvascular basement membranes in diabetes mellitus. J. Pathol. *200*, 537–546.

Uemura, A., Ogawa, M., Hirashima, M., Fujiwara, T., Koyama, S., Takagi, H., Honda, Y., Wiegand, S.J., Yancopoulos, G.D., and Nishikawa, S. (2002). Recombinant angiopoietin-1 restores higher-order architecture of growing blood vessels in mice in the absence of mural cells. J. Clin. Invest. *110*, 1619–1628.

Wachsberger, P., Burd, R., and Dicker, A.P. (2003). Tumor response to ionizing radiation combined with antiangiogenesis or vascular targeting agents: Exploring mechanisms of interaction. Clin. Cancer Res. *9*, 1957–1971.

Willett, C.G., Boucher, Y., di Tomaso, E., Duda, D.G., Munn, L.L., Tong, R.T., Chung, D.C., Sahani, D.V., Kalva, S.P., Kozin, S.V., et al. (2004). Direct evidence that the VEGF-specific antibody bevacizumab has antivascular effects in human rectal cancer. Nat. Med. *10*, 145–147.

Yuan, F., Salehi, H.A., Boucher, Y., Vasthare, U.S., Tuma, R.F., and Jain, R.K. (1994). Vascular permeability and microcirculation of gliomas and mammary carcinomas transplanted in rat and mouse cranial windows. Cancer Res. *54*, 4564–4568.

Yuan, F., Chen, Y., Dellian, M., Safabakhsh, N., Ferrara, N., and Jain, R.K. (1996). Time-dependent vascular regression and permeability changes in established human tumor xenografts induced by an anti-vascular endothelial growth factor/vascular permeability factor antibody. Proc. Natl. Acad. Sci. USA *93*, 14765–14770.

Zips, D., Krause, M., Hessel, F., Westphal, J., Bruchner, K., Eicheler, W., Dorfler, A., Grenman, R., Petersen, C., Haberey, M., and Baumann, M. (2003). Experimental study on different combination schedules of VEGF-receptor inhibitor PTK787/ZK222584 and fractionated irradiation. Anticancer Res. *23*, 3869–3876.